APL Materials

Design of BCP buffer layer for inverted perovskite solar cells using ideal factor

Cite as: APL Mater. **7**, 031117 (2019); https://doi.org/10.1063/1.5087796
Submitted: 04 January 2019 • Accepted: 04 March 2019 • Published Online: 27 March 2019

Naoyuki Shibayama, Hiroyuki Kanda, Tae Woong Kim, et al.

Design of BCP buffer layer for inverted perovskite solar cells using ideal factor

Cite as: APL Mater. 7, 031117 (2019); doi: 10.1063/1.5087796
Submitted: 4 January 2019 • Accepted: 4 March 2019 •
Published Online: 27 March 2019

Naoyuki Shibayama,[1,2,a] Hiroyuki Kanda,[1] Tae Woong Kim,[2] Hiroshi Segawa,[2] and Seigo Ito[1,a]

AFFILIATIONS

[1] Department of Materials and Synchrotron Radiation Engineering, Graduate School of Engineering, University of Hyogo, 2167 Shosha, Himeji 671-2280, Japan

[2] Department of General Systems Studies, Graduate School of Arts and Sciences, The University of Tokyo, 3-8-1 Komaba, Meguro-ku, Tokyo 153-8902, Japan

Note: This paper is part of the special topic on Perovskite Semiconductors for Next Generation Optoelectronic Applications.
[a] **Authors to whom correspondence should be addressed:** itou@eng.u-hyogo.ac.jp and naoyuki.shibayama81@gmail.com

ABSTRACT

In the inverted structure perovskite solar cells, a buffer layer is generally used at the interface between the n-type semiconductor layer and the metal electrode, but its design guidelines have not yet been established. Here, a series of inverted perovskite solar cells have been fabricated with the controlled thickness of bathocuproine (BCP) buffer layers deposited by thermal evaporation and validated the BCP buffer layer evaluation tool. The ideal factor was calculated from the gradient in the plot of *Voc* against the log of *Jsc*, and the effect of the BCP buffer layer on charge recombination was verified. Since the ideal factor greatly decreased from 5 to 1.4 by introducing the BCP buffer layer, it was confirmed that the interface between the n-type semiconductor layer and the metal electrode gradually changed from a Schottky barrier diode to an ohmic contact. On the other hand, it was found that an excessive BCP film thickness causes the series resistance to increase and induced recombination. Finally, as a result of optimizing the perovskite layer and the BCP buffer layer, respectively, the performance exceeding 17% was obtained. This study provides insight into the improvements in the conversion efficiency of perovskite solar cells by optimizing the thickness of the buffer layer using the ideal factor.

Extensive studies on the improvement of the efficiency of organometal halide perovskite solar cells (PSCs) have been carried out during the last decade because PSCs are regarded as promising alternatives to silicon-based photovoltaic devices.[1–3] Since the first PSCs with 3.8% were reported by Miyasaka and co-workers,[4] the PSCs conversion efficiency has reached above 23%.[5] This surprising performance improvement is due to the excellent optical and electrical properties of the organometal halide perovskite materials, such as high absorption coefficient, long carrier diffusion length, and low recombination rate.[6–8] Furthermore, their excellent properties enable variable device architectures ranging from mesoscopic to planar structures with either n-i-p (conventional type) or p-i-n (inverted type) layouts.[9] To improve the conversion efficiency of PSC, it is required to efficiently charge-separate electrons and holes generated in the perovskite layer. In n-i-p PSCs, hole transport layers such as 2,2,7,7-tetrakis(*N*,*N*-di-*p*-methoxyphenylamine)-9,9-spirobifluorene (Spiro-OMeTAD) and Poly[bis(4-phenyl) (2,5,6-trimethylphenyl)amine] (PTAA) are used to efficiently extract the holes between the perovskite layer and the metal electrode. By contrast, fullerene (C60), [6,6]-Phenyl-C_{61}-Butyric Acid Methyl Ester (PCBM) and derivatives are used as the electron transport layer in the p-i-n PSCs,[10–13] which require the buffer layer such as bathocuproine (BCP),[14–17] LiF,[18,19] polyethylenimine (PEIE),[20] tris-(8-hydroxyquinoline) aluminum (Alq_3),[21] SnO_x,[22,23] and $Ti(Nb)O_x$[11] to prevent recombination between the electron transport layer and the metal electrode for high performance. Seo *et al.* reported an improvement in the performance by optimizing the film thickness of LiF used as a buffer layer.[18] The BCP buffer layer can also improve solar cell performance after optimizing the film thickness.[16,17]

However, although it is recognized that film thickness optimization of the buffer layer is important for improving the efficiency, other guidelines for the buffer layer in the PSCs remain unclear.

The ideal factor is a non-destructive technique for examining electrochemical devices using differences in recombination of the diode device.[24] In particular, by using the Suns-Voc method, the measurement taken by changing the incident intensity, it is possible to directly evaluate the recombination current and diffusion current occurring at the semiconductor junction interface by eliminating the influence of series resistance.[25] By using this method, it becomes possible to quantify the effect of the buffer layer.

In this study, we investigated the influence of the BCP buffer layer with different film thicknesses on the charge recombination of PSCs using an ideal factor. By using a thin perovskite layer, it can be confirmed by emphasizing the effect of charge recombination between the PCBM layer and the Ag electrode at the introduction of the BCP layer. Optimized devices optimized perovskite layer achieved 17.2% of PSC. Here, we present it to provide a buffer layer design tool.

The device structure used in this work is FTO/NiOx/$CH_3NH_3PbI_3$/PCBM/BCP/Ag [see Fig. 1(a)]. The $CH_3NH_3PbI_3$ perovskite layers of different film thicknesses were produced as previously reported in Refs. 26–28, with film thicknesses of 200 nm and 550 nm, respectively [Fig. 1(b) and Fig. S1 of the supplementary material]. From the results of cross-sectional scanning electron microscopy (SEM), the film thickness of the BCP layer could not be determined. In reciprocal lattice mapping using wide-angle X-ray scattering (WAXS) (Fig. S2), the peak indicating to the perovskite crystal was observed in a ring shape, so the grains of perovskite crystal were randomly oriented. Furthermore, the perovskite layer has a tetragonal structure since the 211, 202, 123, 204, and 312 reflections, which cannot be seen with the cubic structure, were observed (Fig. S2). A series of PSCs have been fabricated with the controlled thickness of BCP buffer layers deposited by thermal evaporation.

First, the thin perovskite layer (200 nm) was used to confirm the influence of the film thickness of the BCP buffer layer on the PSCs in detail. As summarised in Table I, the conversion efficiency of the inverted PSCs improved with increasing BCP buffer layer until 2 nm. This efficiency improvement is mainly ascribable to the improvement of the *Jsc* and *FF* value. On the other hand, it was found that the conversion efficiency and *Voc* of PSC decreased as the thickness of the BCP buffer layer was above 5 nm.

In order to discuss the origin of the improvement in efficiency, we measured the intensity dependence of *Voc* for the devices with different BCP buffer layer thicknesses. By investigating the change in the ideal factor (n_{id}), the effect of film thickness of the BCP layer on charge transfer was discussed. From the current-voltage characteristics based on the equivalent circuit model, the n_{id} value is given as follows:

$$J(V) = J_{ph} - J_0\left\{\exp\left[\frac{q(V + JR_s)}{n_{id}kT}\right] - 1\right\} - \frac{V + JR_s}{R_{sh}}, \quad (1)$$

where k_B is the Boltzmann constant, T is temperature, q is the elementary charge, *Jph* is the photocurrent, and J_0 is the saturation current density at reverse bias. In the Suns-Voc method, *Jsc* indicates V = 0 and *Voc* indicates *J(V)* = 0

$$J(V = 0) = J_{sc} = J_{ph} - J_0\left\{\exp\left[\frac{qJ_{sc}R_s}{n_{id}kT}\right] - 1\right\} - \frac{J_{sc}R_s}{R_{sh}}, \quad (2)$$

$$J(V) = 0 = J_{ph} - J_0\left\{\exp\left[\frac{qV_{oc}}{n_{id}kT}\right] - 1\right\} - \frac{V_{oc}}{R_{sh}}. \quad (3)$$

From Eqs. (1)–(3), the following equation can be inferred:

$$J_{sc} = J_0\left\{\exp\left[\frac{qV_{oc}}{n_{id}kT}\right] - 1\right\} + \frac{V_{oc}}{R_{sh}} - J_0\left\{\exp\left[\frac{qJ_{sc}R_s}{n_{id}kT}\right] - 1\right\} - \frac{J_{sc}R_s}{R_{sh}}. \quad (4)$$

Equation (4) is the characteristic equation of *Voc*–*Jsc* obtained by the Suns-Voc method, and Jsc and Voc are the functions of the light intensity to be irradiated. In case *Jsc* × *Rs* is smaller than *Voc*, the following equation is obtained:

$$\mathrm{Voc} = \frac{n_{id}kT}{q}\ln\left(\frac{J_{sc}}{J_0}\right). \quad (5)$$

Thus, the calculation of the ideal factor using the Suns-Voc method is not affected by the series resistance, but it is necessary to use a condition where the light intensity is sufficiently strong. Here, the current flowing through the semiconductor depletion layer dominates the diode current. For a single heterojunction model, the direct recombination provides an ideal factor of 1 and the Shockley-Read Hall (SRH) recombination gives an ideal factor of 2 under typical p-n junction solar cells. In general, both direct and SRH recombinations exist simultaneously, and therefore, the parameter of the ideal factor for solar cells is in the range of 1–2.[29,30] On the other hand, it is reported that the ideal factor becomes a value of above 2 in PSCs.[30,31]

Here, we analyzed the effect of the BCP buffer layer on solar cell characteristics using the ideal factor. The ideal factor is calculated using the slope of the plot of *Voc* versus the logarithm of *Jsc* shown in Fig. 2 and Eq. (5). The n_{id} decreased from 5.0 to 1.4 due to

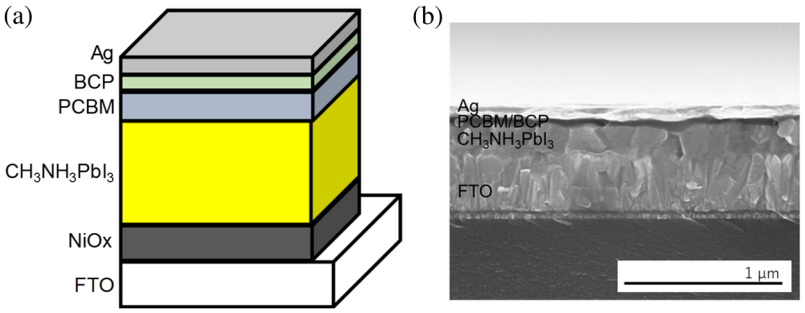

FIG. 1. (a) The structure of FTO/NiOx/$CH_3NH_3PbI_3$/PCBM/BCP/Ag. (b) A cross-sectional scanning electron microscopy (SEM) image of the inverted PSCs with thin $CH_3NH_3PbI_3$ (200 nm) and 2 nm BCP buffer layer.

TABLE I. Characteristics of inverted PSCs using the thin film perovskite layer.

BCP layer	Scan direction	J_{SC} (mA cm^{-2})	V_{OC} (V)	*FF* [. . .]	η (%)	Series resistance (Ω cm^2)	Parallel resistance (Ω cm^2)	Ideal factor
w/o	Forward	9.03	1.08	0.351	3.42	4.7×10^1	3.1×10^2	3.62
	Reverse	8.26	1.05	0.346	3.01	5.3×10^1	2.1×10^2	4.95
1 nm	Forward	13.8	1.07	0.454	6.68	2.4×10^1	3.1×10^2	2.68
	Reverse	13.7	1.07	0.457	6.70	2.4×10^1	2.6×10^2	1.93
2 nm	Forward	18.5	1.06	0.554	10.8	3.7	8.4×10^2	1.64
	Reverse	18.5	1.07	0.549	10.8	3.6	6.9×10^2	1.38
5 nm	Forward	17.9	1.00	0.505	9.06	4.4	2.5×10^2	2.69
	Reverse	17.8	0.867	0.604	9.31	6.2	5.4×10^2	2.22

the incorporation of the BCP buffer layer. A typical Schottky barrier diode exists at the interface between PCBM (organic semiconductors) and Ag (metal),[32] in which the introduction of the BCP layer changes the Schottky barrier diode to an ohmic contact. The PSC without the BCP layer is a model having an additional diode in addition to a diode of PCBM/Ag contributing to photoconversion in an equivalent circuit, which is the cause of making the ideal factor above 2.[31,33,34]

By increasing the film thickness of the BCP buffer layer, the ideal factor gradually decreases. The BCP buffer layer can prevent contact between the PCBM layer and the Ag layer and improves the interface to a good ohmic contact (Fig. 3). By contrast, when the unnecessarily thick BCP buffer layer is used, charge recombination tends to occur at the perovskite/PCBM interface as the resistance at the BCP layer increases.[32] The ideal factor calculated using the *Voc* plotted against *Jsc* logarithm makes it possible to evaluate the BCP layer sharply as it avoids the influence of series resistance. In other words, this method can be used to verify the effect of the passivation layer, which cannot be observed directly by cross-sectional SEM.

Further detailed investigation on hysteresis was done using the ideal factor. The ideal factor varies with the sweep direction of the *J-V* curve, which is mainly due to the difference in the *Voc* value. This directly observes the essence of hysteresis. Therefore, it is

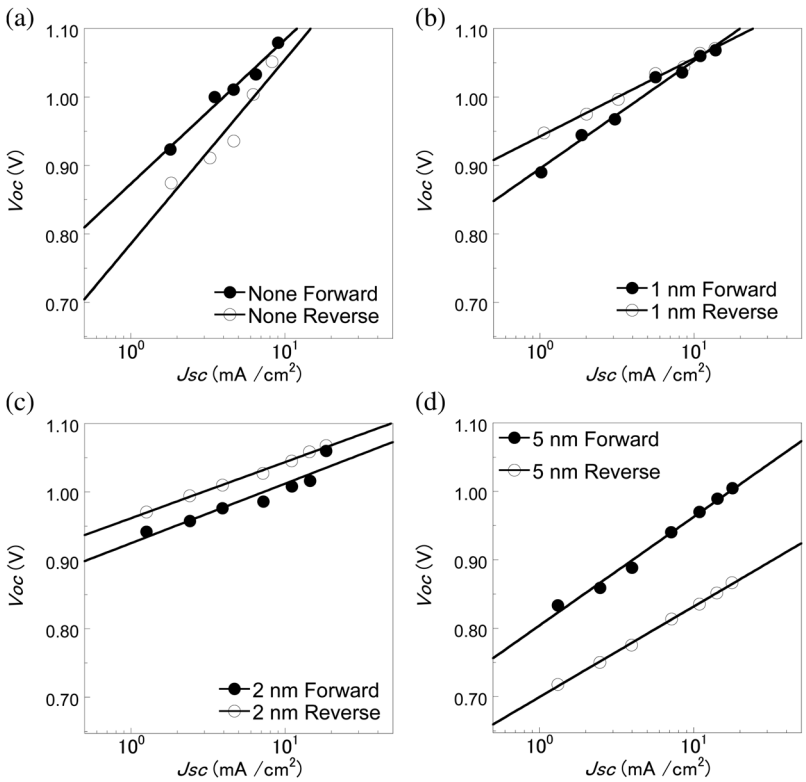

FIG. 2. *Voc* plotted against the logarithm of *Jsc* in the PSCs with a BCP film thickness of (a) none, (b) 1 nm, (c) 2 nm, and (d) 5 nm: the forward scan (close circles) and the reverse scan (open circles).

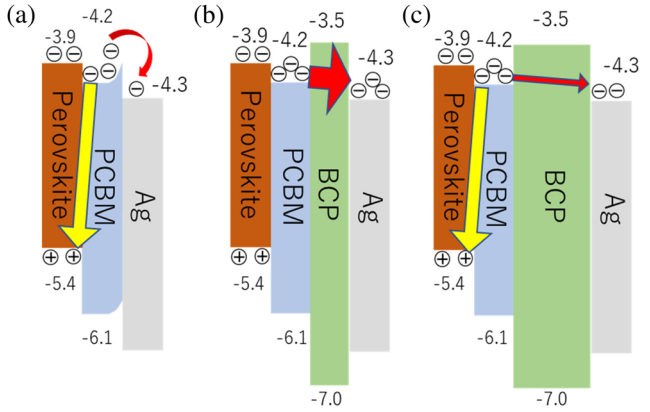

FIG. 3. Energy diagram and charge transfer mechanism: (a) PCBM and Ag are in direct contact, and the interface is the Schottky barrier diode. (b) The BCP buffer layer was inserted at the interface between PCBM and Ag and turned into ohmic contact. (c) An excessive BCP buffer layer is present at the interface between PCBM and Ag, causing recombination between the PCBM and the perovskite layer.

considered that the ideal factor peculiar to the PSC is between n_{id} (forward) and n_{id} (reverse).

Finally, we fabricated the highly efficient inverted PSCs (Fig. S1) using the optimized film thickness of the perovskite layer (550 nm). By using this perovskite layer, 17.2% conversion efficiency was obtained in inverted PSCs as *Jsc* and *FF* were mainly improved (Fig. 4). The value of the ideal factor increased when the perovskite layer was thick, even with the same BCP buffer layer. BCP changes the junction of the interface between PCBM and the metal from a Schottky to an ohmic junction. Therefore, this increase in the ideal factor is mainly affected by the perovskite layer film thickness. From the above, the increase in the perovskite layer film thickness leads to the improvement of the conversion efficiency, but the value of the ideal factor also becomes large because recombination is likely to occur. By using the ideal factor, recombination can be evaluated independently of the conversion efficiency. This result clearly indicates that it is a useful tool to obtain the ideal factor that can quantify the charge recombination at the p-n junction, which optimizes the functional layer and the state of the semiconductor layer that cannot be directly observed.

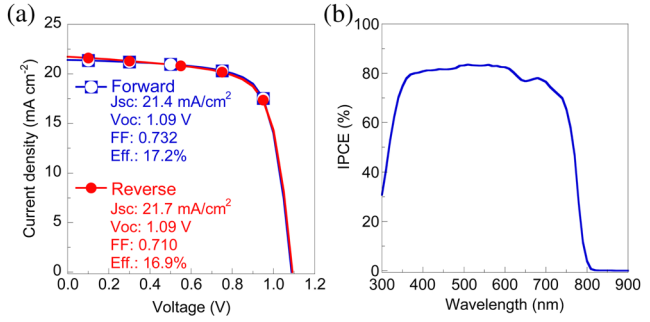

FIG. 4. (a) *J-V* curves and (b) IPCE spectra of PSCs using thick perovskite layers.

In summary, we have demonstrated that it is possible to quantify the film thickness of the BCP buffer layer which is too thin to be observed directly at the PCBM/Ag interface using the ideal factors. The usefulness of this method can be used not only for the evaluation of the buffer layer, but also for the interface treatment such as the passivation treatment.

See supplementary material for details of fabrication of perovskite devices. Additional information of WAXS (XRD) pattern of perovskite layer, cross-section SEM and the Ideal factor of the best cell.

This work was supported by New energy and industrial Technology Development Organization (NEDO), Japan. The authors thank Y. Nakamura (The University of Tokyo, Japan), Dr. S. Yasuno, and Dr. T. Koganezawa (Japan Synchrotron Radiation Research Institute) for discussions. N.S. sincerely thanks the Nanotechnology Platform (Project No. NPS17072) by Nara Institute of Science. The WAXS measurement was performed at SPring-8 BL19B2 and BL46XU with the approval of the Japan Synchrotron Radiation Research Institute (JASRI, Proposal Nos. 2018B1809, 2018B1855, 2018B1862, and 2018B1868).

REFERENCES

[1] T. Miyasaka, Bull. Chem. Soc. Jpn. **91**, 1058 (2018).
[2] W. A. Dunlap-Shohl, Y. Zhou, N. P. Padture, and D. B. Mitzi, Chem. Rev. **119**, 3193 (2019).
[3] S. Ito, APL Mater. **4**, 091504 (2016).
[4] A. Kojima, K. Teshima, Y. Shirai, and T. Miyasaka, J. Am. Chem. Soc. **131**, 6050 (2009).
[5] M. A. Green, Y. Hishikawa, E. D. Dunlop, D. H. Levi, J. Hohl-Ebinger, M. Yoshita, and A. W. Y. Ho-Baillie, Prog. Photovolt.: Res. Appl. **27**, 3 (2019).
[6] A. Paulke, S. D. Stranks, J. Kniepert, J. Kurpiers, C. M. Wolff, N. Schön, H. J. Snaith, T. J. K. Brenner, and D. Neher, Appl. Phys. Lett. **108**, 113505 (2016).
[7] L. K. Ono, E. J. Juarez-Perez, and Y. Qi, ACS Appl. Mater. Interfaces **9**, 30197 (2017).
[8] W. Li, Z. Wang, F. Deschler, S. Gao, R. H. Friend, and A. K. Cheetham, Nat. Rev. Mater. **2**, 16099 (2017).
[9] J. Nakazaki and H. Segawa, J. Photochem. Photobiol. C. **35**, 74 (2018).
[10] D. Luo, W. Yang, Z. Wang, A. Sadhanala, Q. Hu, R. Su, R. Shivanna, G. F. Trindade, J. F. Watts, Z. Xu, T. Liu, K. Chen, F. Ye, P. Wu, L. Zhao, J. Wu, Y. Tu, Y. Zhang, X. Yang, W. Zhang, R. H. Friend, Q. Gong, H. J. Snaith, and R. Zhu, Science **360**, 1442 (2018).
[11] W. Chen, Y. Wu, Y. Yue, J. Liu, W. Zhang, X. Yang, H. Chen, E. Bi, I. Ashraful, M. Grätzel, and L. Han, Science **350**, 944 (2015).
[12] W. Chen, F.-Z. Liu, X.-Y. Feng, A. B. Djurišić, W. K. Chan, and Z.-B. He, Adv. Energy Mater. **7**, 1700722 (2017).
[13] B. G. H. M. Groeneveld, M. Najafi, B. Steensma, S. Adjokatse, H.-H. Fang, F. Jahani, L. Qiu, G. H. T. Brink, J. C. Hummelen, and M. A. Loi, APL Mater. **5**, 076103 (2017).
[14] J.-Y. Jeng, Y.-F. Chiang, M.-H. Lee, S.-R. Peng, T.-F. Guo, P. Chen, and T.-C. Wen, Adv. Mater. **25**, 3727 (2013).
[15] N. Shibayama, S. Fukumoto, H. Sugita, H. Kanda, and S. Ito, Mater. Res. Bull. **106**, 433 (2018).
[16] C. Chen, S. Zhang, S. Wu, W. Zhang, H. Zhu, Z. Xiong, Y. Zhang, and W. Chen, RSC Adv. **7**, 35819 (2017).
[17] D.-X. Yuan, X.-D. Yuan, Q.-Y. Xu, M.-F. Xu, X.-B. Shi, Z.-K. Wang, and L.-S. Liao, Phys. Chem. Chem. Phys. **17**, 26653 (2015).
[18] J. Seo, S. Park, Y. C. Kim, N. J. Jeon, J. H. Noh, S. C. Yoon, and S. I. Seok, Energy Environ. Sci. **7**, 2642 (2014).

[19]X. Liu, H. Yu, L. Yan, Q. Dong, Q. Wan, Y. Zhou, B. Song, and Y. Li, ACS Appl. Mater. Interfaces **7**, 6230 (2015).
[20]H. Zhang, H. Azimi, Y. Hou, T. Ameri, T. Przybilla, E. Spiecker, M. Kraft, U. Scherf, and C. J. Brabec, Chem. Mater. **26**, 5190 (2014).
[21]L. J. Chen, G. Wang, L. B. Niu, Y. Q. Yao, Y. X. Guan, Y. T. Cui, and Q. L. Song, RSC Adv. **8**, 15961 (2018).
[22]Z. Zhu, Y. Bai, X. Liu, C.-C. Chueh, S. Yang, and A. K.-Y. Jen, Adv. Mater. **28**, 6478 (2016).
[23]Y. Wang, C. Duan, J. Li, W. Han, M. Zhao, L. Yao, Y. Wang, C. Yan, and T. Jiu, ACS Appl. Mater. Interfaces **10**, 20128 (2018).
[24]C. Zhang, J. Zhang, Y. Hao, Z. Lin, and C. Zhu, J. Appl. Phys. **110**, 064504 (2011).
[25]S. H. Lim, K. O'Brien, E. H. Steenbergen, J.-J. Li, D. Ding, and Y.-H. Zhang, in *Proceedings of the 35th IEEE Photovoltaic Specialists Conference* (IEEE, 2010), p. 712.
[26]H. Kanda, N. Shibayama, A. Uzum, T. Umeyama, H. Imahori, K. Ibi, and S. Ito, ACS Appl. Mater. Interfaces **10**, 35016 (2018).
[27]H. Kanda, N. Shibayama, A. Uzum, T. Umeyama, H. Imahori, Y.-H. Chiang, P. Chen, M. K. Nazeeruddin, and S. Ito, Mater. Today Energy **7**, 190 (2018).
[28]N. Shibayama, H. Kanda, S. Yusa, S. Fukumoto, A. K. Baranwal, H. Segawa, T. Miyasaka, and S. Ito, Nano Convergence **4**, 18 (2017).
[29]C. Li, Z. Song, D. Zhao, C. Xiao, B. Subedi, N. Shrestha, M. M. Junda, C. Wang, C.-S. Jiang, M. Al-Jassim, R. J. Ellingson, N. J. Podraza, K. Zhu, and Y. Yan, Adv. Energy Mater. **9**, 180315 (2018).
[30]H. D. Kim, H. Ohkita, H. Benten, and S. Ito, Adv. Mater. **28**, 917 (2016).
[31]P. Liao, X. Zhao, G. Li, Y. Shen, and M. Wang, Nano-Micro Lett. **10**, 5 (2018).
[32]K. Miyano, N. Tripathi, M. Yanagida, and Y. Shirai, Acc. Chem. Res. **49**, 303 (2016).
[33]G. L. Araujo, E. Sánchez, and M. Martí, Sol. Cells **5**, 199 (1982).
[34]K. Nishioka, N. Sakitani, Y. Uraoka, and T. Fuyuki, Sol. Energy Mater. Sol. Cells **91**, 1222 (2007).